Pergamon

Int. J. Heat Mass Transfer. Vol. 40, No. 13, pp. 3049–3058, 1997

Printed in Great Britain
0017-9310/97 $17.00+0.00

PII: S0017-9310(96)00378-X

A photothermal method with step heating for measuring the thermal diffusivity of anisotropic solids

A. GRIESINGER,† W. HURLER‡ and M. PIETRALLA§

Abteilung für Experimentelle Physik, Universität Ulm, Albert-Einstein-Allee 11, D-89069 Ulm, Germany

(*Received* 15 *April* 1996 *and in final form* 16 *October* 1996)

Abstract—A pure radiative method is presented for measuring the directionally-dependent thermal diffusivities of anisotropic solids, especially of free-standing films. A real point and line source are realized by a focussed laser beam. Both configurations allow measurements of the anisotropic thermal diffusivity. Because of the smaller power density applied for the line source, this method is very suited for thermic sensitive films. Virtual image sources are used to account for the boundary conditions of a rectangular slab. The temperature vs time curves are recorded by infrared radiation using an InSb-detector. They are fitted to the solution for a constant heat source switched on at time zero (step heating) disregarding the prefactor. Thus, there is no need to know the absorption coefficient or the absolute temperature rise of the sample. The influence of sample dimensions and of radiative losses is investigated. For sufficiently thin samples a two-dimensional treatment is suited. Extrapolating the diffusivities determined in different time spans to zero heating time excludes radiation losses. A comparison to results from steady-state methods for well-defined samples confirm the reliability of the method. Representative results on highly oriented polymers are presented. © 1997 Elsevier Science Ltd.

1. INTRODUCTION

In this paper we present a method for measuring the directionally-dependent thermal diffusivity of low conducting materials such as polymers. In that case periodic methods using thermal waves suffer from the high damping due to the low thermal diffusivity. Moreover, the mixing of tensor components makes the analysis difficult and thus, the appropriate methods are not well developed up to now [1]. This is surprising since heat conduction was the first solid state property, except the polarization dependent refractive index, whose directional dependence was discovered by De Sénarmont [2, 3]. From a present point of view the method was quite modern by imaging the isotherms due to a heat point source. A thin layer of paraffin wax on a crystal surface recorded the isotherms by the border between the molten and recrystallized part around the heat source and the exterior solid part. He observed circles and ellipses as isotherms. For the latter the anisotropy ratio

$$A = \frac{k^{\parallel}}{k^{\perp}} = \frac{\alpha^{\parallel}}{\alpha^{\perp}} = \left(\frac{x^{\parallel}}{x^{\perp}}\right)^2 \tag{1}$$

follows from the ratio of the principal axes $x^{\parallel}$, $x^{\perp}$ of the ellipsis. He found e.g. for a quartz crystal plate $A = 1.72$ which is comparable to $A = 1.72 \pm 0.3$ from data taken from [4] or $A = 1.70 \pm 0.1$ from a refined version of the method [5]. In addition, he tried successfully to find whether mechanical stress applied to a glass could result in anisotropic heat conduction.

The method was improved by Roentgen [6] using evaporation of a moisture film freshly deposited onto the surface. Spores (lycopodium) were subsequently spread over the sample and blown away. They remained attached at the wet part and marked a very accurate isotherm.

One of the main problems at that time was to establish the symmetry of the thermal conductivity tensor [6], which is an important question from a principle point of view. Since the methods used delivered only relative values, despite their high sensitivity in a small temperature range, they were more or less forgotten. Müller assisting Debye with experiments during the lectures demonstrated this method and later applied it to oriented polymers [7]. In polymers the anisotropy can be easily changed by orienting the linear macromolecules within a sample by simply stretching it uniaxially. The anisotropy can serve as a measure of orientation if birefringence is not measurable. With the advent of liquid crystals these have been used as temperature indicators. Anisotropies up to $A = 25$ have been recorded for linear polyethylene at room temperature [8]. When infrared detectors became available, the method could be treated by electronic

†Present address: Universität Stuttgart, Institut für Thermodynamik und Wärmetectnik, Pfaffenwaldring 6 D-70550, Stutgart, Germany.

‡Present address: debis Systemhaus GEI, Magirusstr. 43, 89077 Ulm, Germany.

§Author to whom correspondence should be addressed.

NOMENCLATURE

$A = \alpha_{\parallel}/\alpha^{\perp}$ anisotropy ratio
b sample width
c_p specific heat at constant pressure
d sample thickness
E_1 exponential integral function
erf error function
erfc 1-erf
f frequency
h height of image sources above sample surface
$k, k^{\parallel}, k^{\perp}$ thermal conductivity, parallel, perpendicular to symmetry axis
N dimension of space (2,3)
p pressure
$\hat{Q}$ specific power of heat sources
r distance thermometer spot/heating spot
r_0 radius of the source spot
R geodesic distance
s slope
t time
T temperature
$\mathbf{x}$ space vector
x_i, y spatial coordinates
X_c fractional crystallinity.

Greek symbols
$\alpha, \alpha^{\parallel}, \alpha^{\perp}$ thermal diffusivity, parallel, perpendicular to symmetry axis
α_{ij}, α^{ij} tensor components of thermal diffusivity
$\lambda = L/L_0$ draw ratio or wavelength
μ penetration depth
ρ density
$\xi = R^2/t$.

means and thus, used in the purely transient regime of heat conduction.

A first step in this direction was made in Ref. [5] where it was shown, that the anisotropy ratio follows from the ratio of the slopes of $T(t)$-curves due to a step heating point source:

$$\frac{s(x_1)}{s(x_2)} = \left(\frac{x_1}{x_2}\right)^N A^{\frac{N}{2}}. \tag{2}$$

x_i: distance of the sensing point from the source into direction i, s: slope at the point of inflection of the $T(t)$ curve, N: dimensionality of the heat equation ($N = 2,3$). In this paper we will present the development of the step heating method now yielding absolute values of directionally-dependent thermal diffusivity. This method is especially well suited for low heat conductors, where time intervals of 10–100 s can be used for recording the $T(t)$-curves with sufficient sensitivity. The radiative temperature scanning enables measurements at high temperatures, but not much below 0°C.

2. THEORY

The heat diffusion equation in the presence of sources is given by

$$\frac{\partial T(\mathbf{x}, t)}{\partial t} - \alpha_{ij}\frac{\partial^2 T(\mathbf{x}, t)}{\partial x_i \partial x_j} = \hat{Q}(\mathbf{x}, t). \tag{3}$$

α_{ij}: component of the diffusivity tensor $\boldsymbol{\alpha} = \mathbf{k}/c_p\rho$ where $\mathbf{k}$ is the thermal conductivity tensor, c_p is the specific heat at constant pressure and ρ the density. $\hat{Q}(\mathbf{x}, t) = \dot{Q}(\mathbf{x}, t)/c_p\rho$ is the specific power of a heat source. A special solution due to a finite amount of energy released in zero time at one point of the sample, i.e. a delta-heat source, is the Green's function of the anisotropic diffusion equation [9]. This solution is approximated by the flash-heating methods. All other solutions due to source distributions in space and time can be derived by appropriate integrations.

$$G_{\alpha}^{N} = \begin{cases} \dfrac{[\det(\alpha^{ij})]^{1/2}}{[4\pi(t-t')]^{\frac{N}{2}}} \exp\left(-\dfrac{R^2(\mathbf{x}, \mathbf{x}')}{t-t'}\right): & t \geq t' \\ 0: & t < t' \end{cases}$$

where

$((\alpha^{ij})) = ((\alpha_{ij}))^{-1}$: inverse tensor of the thermal diffusivity i.e. the thermal resistivity
$R^2(\mathbf{x}, \mathbf{x}') = \frac{1}{4}\alpha^{ij}(x_i - x_i')(x_j - x_j')$: geodesic distance
N: dimension.

In the following we will confine ourselves to two cases: a point source of constant strength and a line source of constant strength. Both are switched on at time $t = 0$ (Fig. 1). In the case of the point source we obtain by integration with respect to time the temperature observed at that time at a point $\mathbf{x}$

$$T(\mathbf{x}, t) = \hat{Q}\frac{\sqrt{[\det(\alpha^{ij})]}}{4\pi}\frac{\operatorname{erfc}\left(\dfrac{R_{PQ}}{\sqrt{t}}\right)}{R_{PQ}} \tag{4}$$

In case of the line source we get by additional one-dimensional integration with respect to space

$$T(\mathbf{x}, t) = \hat{Q}\frac{\sqrt{\alpha^{22}\alpha^{33}}}{2\pi}E_1\left(\frac{\alpha^{22}y^2 + \alpha^{33}d^2}{4t}\right) \tag{5}$$

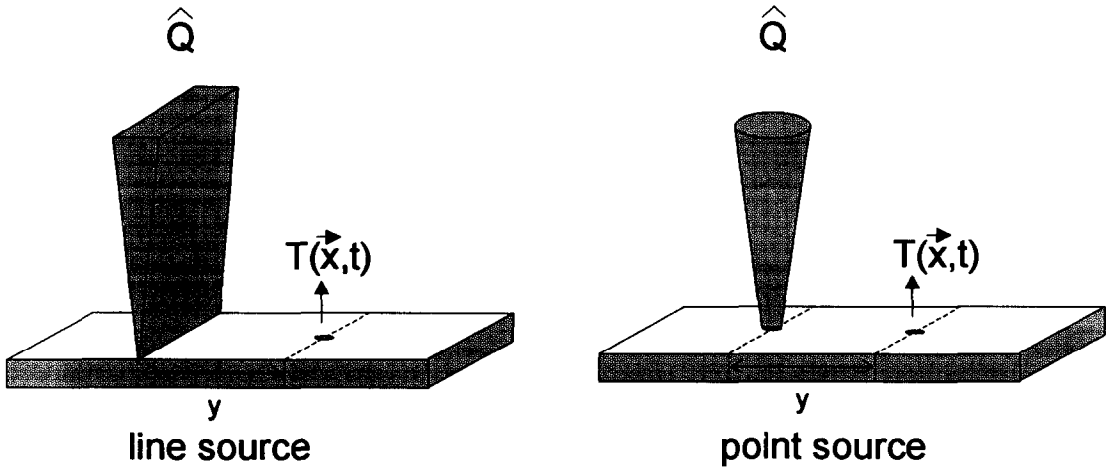

Fig. 1. Schematic configuration of the line and point source (y is the distance of the thermometer spot from the heating spot).

where

$$R_{PQ} = \tfrac{1}{2}\sqrt{\alpha^{11}x^2 + \alpha^{22}(y^2+d^2)}$$

$$\operatorname{erfc}(x) = 1 - \operatorname{erf}(x) = \frac{2}{\sqrt{\pi}}\int_x^\infty e^{-t^2}\,dt$$

erf: error function

$$E_1(x) = \int_x^\infty \frac{e^{-u}}{u}\,du : \text{exponential integral function.}$$

Since isotherms are the loci of constant geodesic distances i.e.

$$\frac{x_1^2}{4\alpha_{11}t} = \frac{x_2^2}{4\alpha_{22}t} \tag{6}$$

we get directly equation (1) for the principal directions. It is obvious that this relation holds in the stationary case as well as in any transient one. From $T(\mathbf{x}) = \text{const}\cdot f(\xi)$ with $\xi = (R^2/t)$ we further see that all curves have the same shape i.e. they follow a mastercurve after proper scaling of the axes. The scaling factor for the time axis is given by the diffusivity. It is determined by a fit of the shape to the measured $T(t)$-curve taken at distance r. Since only the shape is fitted, the strength of the signal depending on the absorption as well as the emissivity and the absolute temperature calibration are of no concern. This is a significant advantage of our treatment. Figure 2 shows the comparison of the normalized temperature traces of a point and a line source described by equations (4) and (5) (calculations with thermal diffusivity $\alpha = 1\cdot 10^{-7}$ m^2/s, distance $y = 2.3$ mm). Despite general simplicity the boundary conditions and experimental details need further consideration.

2.1. *Boundary conditions*

The presence of a flat boundary can be treated using the method of image sources. No heat flux across the surface i.e. no losses to the surrounding is achieved by posing an image of the real source such that the surface acts as a mirror plane. Constant temperature at the surface is achieved by posing an image drain of equal strength at the above mentioned position. This situation might appear for surfaces of bad conductors in close contact to a metal or other good conductor.

Intermediate boundary conditions can be approximated in principle by weighting the images with a factor $-1 \leqslant w \leqslant +1$. We have not tried such an approach because it introduces a further unknown parameter and we doubt in its general usefulness. If there are pairs of surfaces like that of a rectangular slab we must consider the images of either side. Thus, images of images appear resulting in an infinite sum.

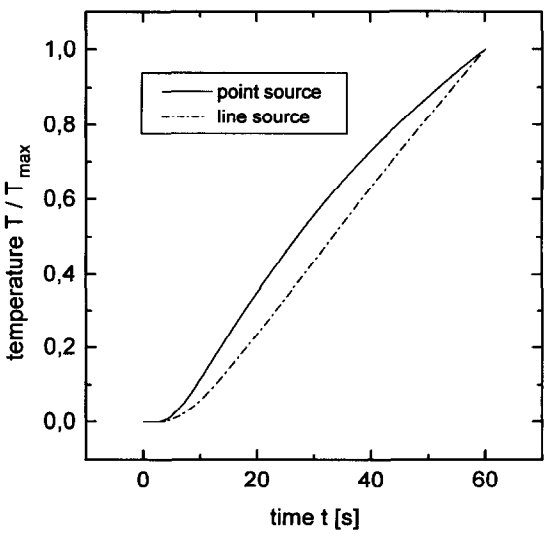

Fig. 2. Comparison of the original temperature trace $T(t)$ from a point source and a line source for $\alpha = 1{*}10^{-7}$m^2/s at a distance $y = 2.5$ mm. The curves are normalized with the value at $t = 60$ s.

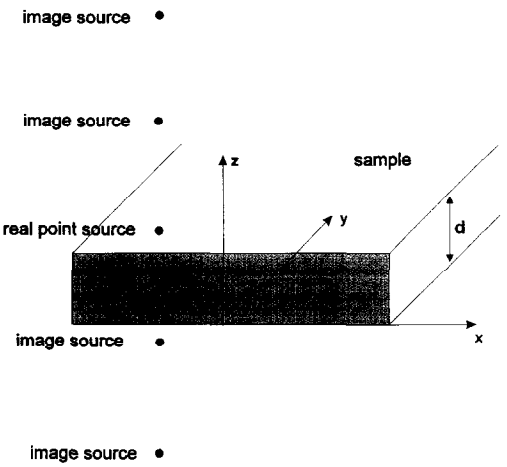

Fig. 3. The principle of image sources. The real point source is reflected at the lower surface ($z = 0$). The resulting image source is reflected at the upper surface ($z = d$). The new two image sources are reflected again at the lower and upper surface, and so on.

For simplification we consider the sample as an infinite slab. This situation is sketched in Fig. 3.

Including the image sources equations (4) and (5) result in

$$T(\mathbf{x},t) = \hat{Q}\frac{\sqrt{[\det(\alpha^{ij})]}}{4\pi}\left(\frac{\operatorname{erfc}\left(\frac{R_{PQ}}{\sqrt{t}}\right)}{R_{PQ}} + \sum_{h_z=1}^{\infty}\frac{\operatorname{erfc}\left(\frac{R_{BQ1}}{\sqrt{t}}\right)}{R_{BQ1}} + \sum_{h_z=1}^{\infty}\frac{\operatorname{erfc}\left(\frac{R_{BQ2}}{\sqrt{t}}\right)}{R_{BQ2}}\right) \quad (7)$$

$$T(\mathbf{x},t) = \hat{Q}\frac{\sqrt{\alpha^{22}\alpha^{33}}}{2\pi}\left(E_1\left(\frac{\alpha^{22}y^2+\alpha^{33}d^2}{4t}\right) + \sum_{h_z=1}^{\infty}E_1\left(\frac{R^*_{BQ1}}{t}\right) + \sum_{h_z=1}^{\infty}E_1\left(\frac{R^*_{BQ2}}{t}\right)\right) \quad (8)$$

where

$$R_{BQ1} = R_{PQ}\sqrt{1+\frac{4h_z(h_z-1)}{\frac{\alpha^{11}}{\alpha^{22}}\left(\frac{x}{d}\right)^2+\left(\frac{y}{d}\right)^2}+1}$$

$$R_{BQ2} = R_{PQ}\sqrt{1+\frac{4h_z(h_z+1)}{\frac{\alpha^{11}}{\alpha^{22}}\left(\frac{x}{d}\right)^2+\left(\frac{y}{d}\right)^2}+1}$$

$$R'_{BQ1} = \alpha^{33}h_z d^2(h_z-1)+\tfrac{1}{4}(\alpha^{22}y^2+\alpha^{33}d^2)$$

$$R'_{BQ2} = \alpha^{33}h_z d^2(h_z+1)+\tfrac{1}{4}(\alpha^{22}y^2+\alpha^{33}d^2).$$

For evaluating our data we posed the source onto the surface. That is the situation, which is most easily obtained experimentally by preparing an absorbing surface. The number of image sources to be summed for fitting the experimental curves depends on the diffusivity and increases dramatically with decreasing sample thickness. The influence of thickness on the number of images is shown in Fig. 4.

As a criterion for ceasing the summation one can use a fixed ratio $\hat{Q}(x)/\hat{Q}(o) < 10^{-3}$ for the source at x compared to the real source at the origin. Alternatively, one can use $\Sigma_i^{2i}\hat{Q}(x_i)/\hat{Q}(o) < 10^{-3}$, which guarantees a smaller error when neglecting higher terms. If the sample thickness approaches zero the number of images goes to infinity. In this case the two-dimensional diffusion equation should be used. Here sums over images are avoided and the numerical fitting becomes much faster on the computer.

2.2. *The two-dimensional problem*

$$\frac{\partial T(\mathbf{x},t)}{\partial t} - \alpha_{ij}\frac{\partial^2 T(\mathbf{x},t)}{\partial x_i\,\partial x_j} = \hat{Q}(\mathbf{x},t), \quad i,j = 1,2. \quad (9)$$

The solution of this equation in case of a point source is given by

$$T(\mathbf{x},t) = \hat{Q}\frac{\sqrt{[\det(\alpha^{ij})]}}{4\pi}E_1\left(\frac{R^2}{t}\right) \quad (10)$$

where

$$R^2 = \tfrac{1}{4}\alpha^{ij}x_i x_j \quad i,j = 1,2. \quad (11)$$

The case of the line source heating a two-dimensional sample corresponds to one-dimensional heat conduction. In this case it is not possible to give an analytical solution of the one-dimensional heat diffusion equation with a heat source switched on at time $t = 0$.

The solution of the two-dimensional diffusion equation is especially suited for sufficiently thin free-standing anisotropic films. What 'sufficiently thin'

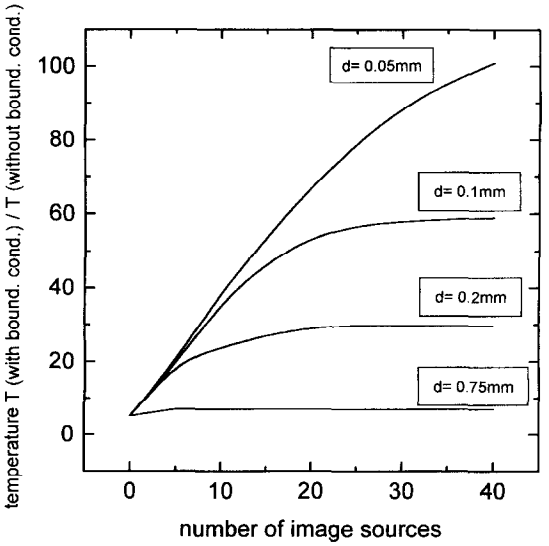

Fig. 4. Temperature T (with bound. cond.)/T (without bound. cond.) vs the number of image sources for different thicknesses d.

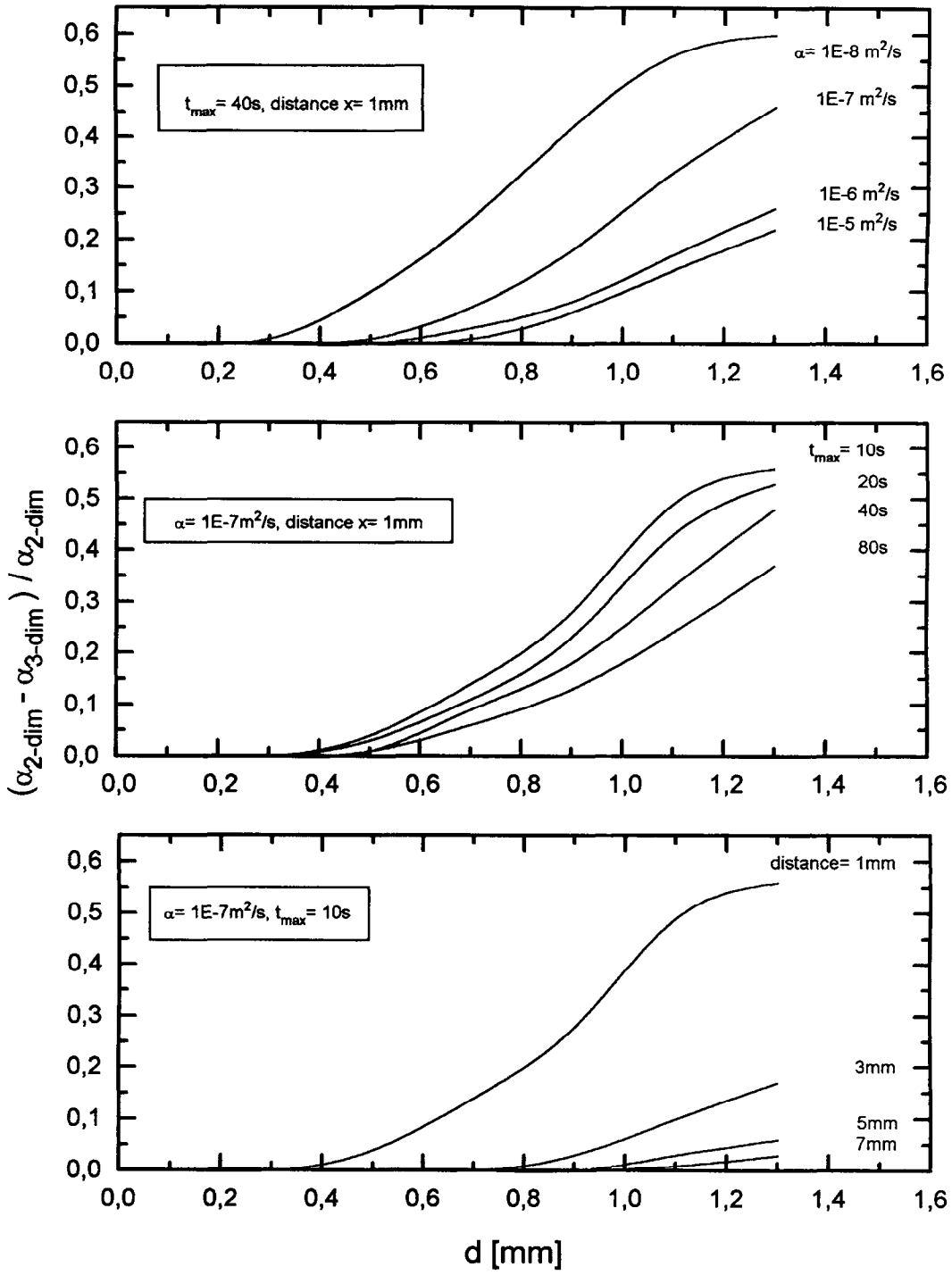

Fig. 5. The influence of sample thickness: calculated three-dimensional $T(t)$-curves fitted with the two-dimensional solution.

means can be tested both theoretically and experimentally. For this purpose we produced master curves $T11(\xi)$ with the number of image sources as a parameter. To these curves the two-dimensional solution is fitted. The results are shown in Fig. 5. The experimental verification is quite obvious. Results obtained with HDPE-samples varying in sample thickness are shown in Fig. 6. From this considerations we infer that for a sample thickness $d \leqslant 0.3$ mm the two-dim treatment is appropriate.

2.3. *Finite sample width*

Since samples are not infinitely wide this influence must be treated as well. It can be solved again with

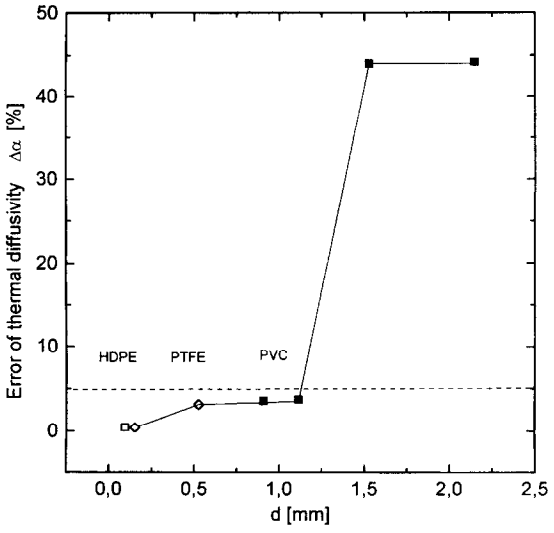

Fig. 6. Experimental investigation of the influence of sample thickness fitted with the two-dimensional point source.

the method of images as well as experimentally by slicing a sample into smaller strips. The experimental investigation of this is shown in Fig. 7. This result does not depend on the absolute magnitude of the diffusivity, which only changes the time scale of data collection, but it depends on the r/b ratio (r is the distance of the thermometer spot from the heating spot, b is the sample width).

2.4. *Finite source extension*

Any experimental verification of the method must use an extended source e.g. the gaussian profile of a focused laser beam. An analytical solution consists of an integration over the intensity distribution of the source, and is only possible in the one-dimensional case. For a constant intensity on a circular surface we

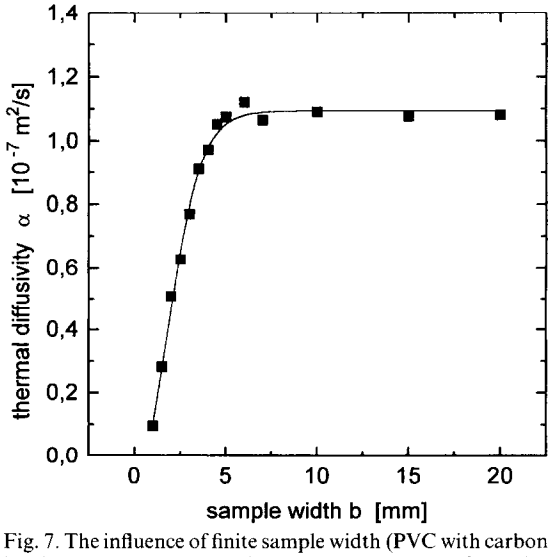

Fig. 7. The influence of finite sample width (PVC with carbon black) on the thermal diffusivity α in the case of a point source.

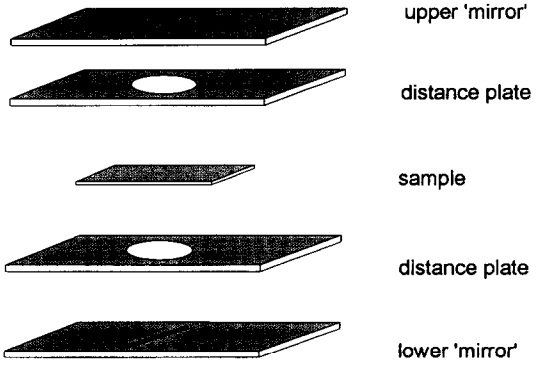

Fig. 8. Experimental setup to reduce radiation losses: polished faces of brass with a gold layer are used as "mirrors".

performed a numerical integration. As a rule we have found that $r/r_0 \geqslant 10$ must hold where r_0 is the radius of the source spot and r the distance of the sensing point from the source. r_0 can also be interpreted as the integral half width of a Gaussian profile i.e. the half width of a cylinder with the same 'volume' (energy flux) as the Gaussian profile.

2.5. *Heat losses to the surrounding*

Heat losses hindering the boundary conditions to be established are due to conduction, convection and radiation. The convection losses are avoided by evacuating the sample compartment. If the pressure is chosen to be $p < 10^{-4}$mbar heat conduction of the remaining air is also negligible.

During any measurement due to the Stefan–Boltzmann T^4-law, radiation losses affect the diffusivities determined dramatically with increasing temperature. Only at low temperatures they can be neglected. In our case the result is a systematical shift of the thermal diffusivity to higher values. The reason is that due to the losses the $T(t)$-curves level off more rapidly than without as do curves for higher diffusivities compared to lower ones. Thus, a fit trying to mimic that shape of the $T(t)$-curve results in a higher thermal diffusivity than is really present.

We have tried to overcome this problem experimentally and by data handling. We placed polished faces of brass covered with a layer of gold close (distance $\leqslant 5$ mm) to the sample surface. Holes ($\phi \sim 0.2$ mm) in case of the point source and a slit in case of the line source ($d \sim 0.2$ mm) were drilled for the source beam and for the sensing radiation (Fig. 8). Thus, heat losses by radiation are reduced.

If no radiation losses are present, results from fits embracing different time spans $[0, t_{max}]$ must group to a horizontal line when plotted vs t_{max}. With radiation losses it must be an increasing curve because losses become more prominent at longer times. We apply a heuristical procedure to exclude the radiation effects. We record the $T(t)$ over a longer time. We then produce N data sets $[0, t_n]$ from it by putting $t_n = t_{max}/n$, $n = 1, \ldots, N$. Each set is used to determine the appar-

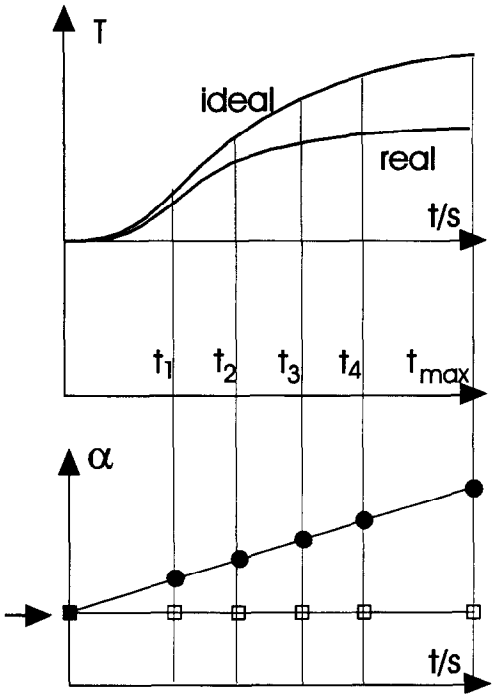

Fig. 9. Extrapolation procedure with T vs t (above) and the resulting α (below). Extrapolation to $t = 0$ s gives the appropriate diffusivity α.

ent diffusivity which is plotted vs t_n (Fig. 9). If a linearly increasing relationship is found an extrapolation to $t \to 0$ yields the diffusivity free from radiation effects.

This is demonstrated in Fig. 10 with a PVC sample: (i) measured with the point source; (ii) measured with a line source. The spread of results is demonstrated

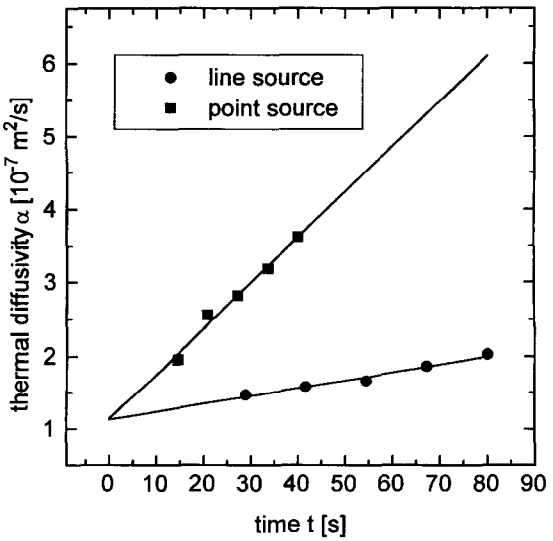

Fig. 10. Apparent thermal diffusivity vs evaluation time for a PVC sample. Extrapolation to $t = 0$ s gives the "true" thermal diffusivity.

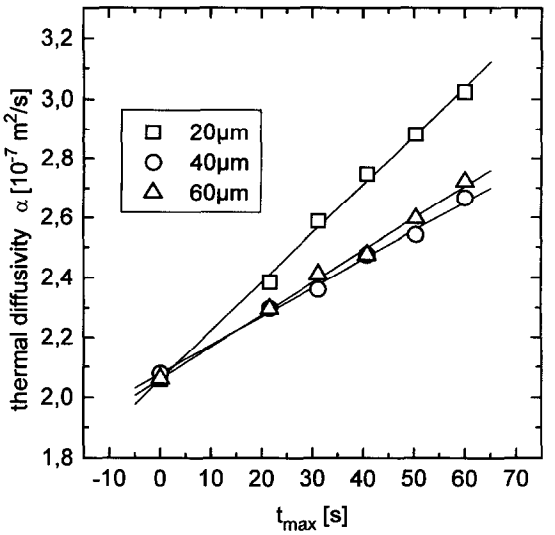

Fig. 11. Extrapolation procedure of an isotropic PE-sample for different sample thicknesses.

by taking temperature records up to different times t_{max} and subsequent data evaluation as just explained. The plot of the extrapolated data belonging to each t_{max} indicates the quality of the results. The influence of decreasing thickness is an enhancement of radiation losses, compared to the total heat content. The curves become steeper as seen in Fig. 11. The extrapolated result remains the same confirming the validity of our treatment.

It is satisfying to note, that the extrapolated values coincide for both methods. Because of the smaller power density of the laser beam in case of the line source the maximum temperature in the sample becomes smaller. Thus, radiation losses decrease, which results in a smaller slope. Even if the slopes of the curves are very different on account of different sample thicknesses they cross at $t = 0$ s. Thus, this procedure appears to be highly reliable.

2.6. *Experimental*

A schematic diagram of the apparatus is shown in Fig. 12. For heating the sample we use a CO_2-laser (λ = 10, 6 μm). To make adjustment easier the invisible beam of the i.r.-laser is combined with the visible beam of a laser-diode.

A shutter is opened at the time $t_0 = 0$ s. The laser–beam, which is turned round and focused by mirrors, heats the rear side of the sample. In case of the line-source the laser-beam is spread to a line. At a distance from about 2 mm from the heating point or line, the heating of the sample is measured with an i.r.-microscope. An InSb-detector in the microscope changes the heat radiation of the sample chopped by a tuning fork into a voltage signal. This signal is filtered with a lock-in amplifier, digitized and stored with a PC.

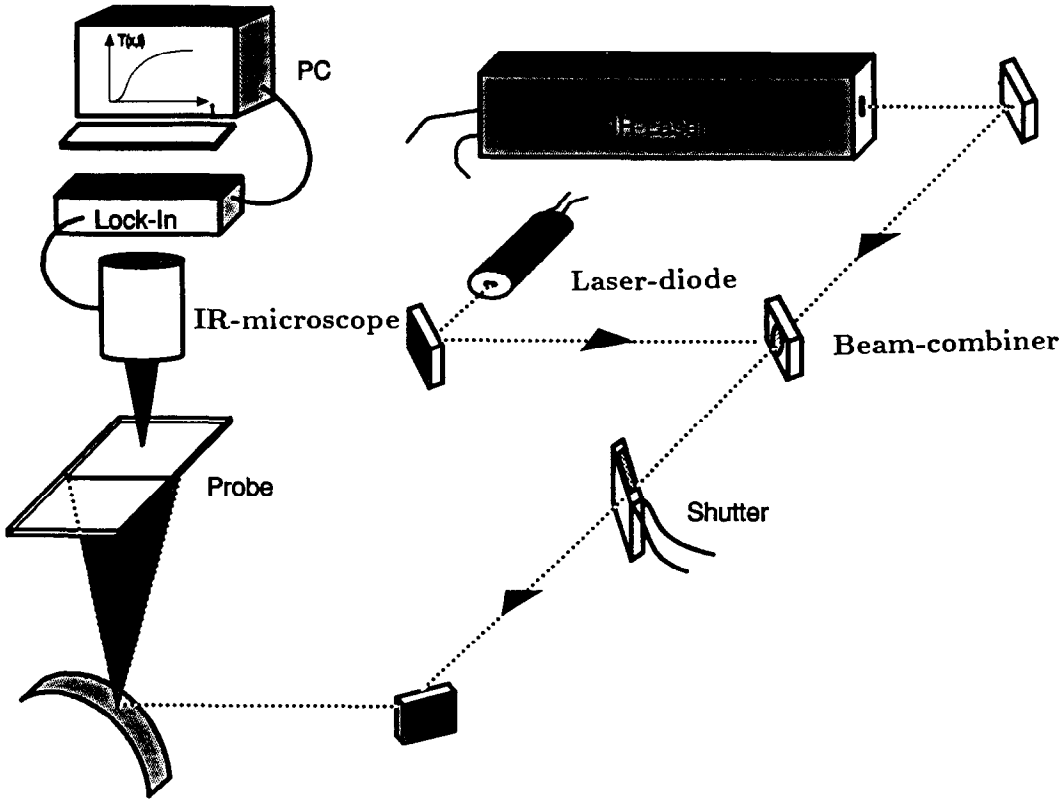

Fig. 12. Schematic diagram of the apparatus.

Table 1. Comparison of the measured thermal diffusivity of PTFE and reactor-steel [13]

PTFE					
T [C]	k [W/mK]	α [10 ^{7}m^2/s]	c_p [J/kgK]	ρ[kg/m^3]	our results α [10 ^{7}m^2/s]
60	0.299	1.36	1035	2121	1.40
180	0.307	1.28	1198	2009	1.25
Reactor steel 1.4970 (× 10NiCrMoTiB15 15)					
T [C]	k [W/mK]	α [10^{-7}m^2/s]	c_p [J/kgK]	ρ[kg/m^3]	our results α [10 ^{7}m^2/s]
60	14.38	36.5	495.5	7951.0	34.7
200	16.53	39.9	524.3	7901.7	38.5

3. COMPARISON TO STEADY-STATE METHODS

The relative accuracy of the method is rather good as can be seen e.g. from Fig. 11. The absolute accuracy is more difficult to determine. For this purpose we measured two samples in an extended temperature range for comparison with steady state methods: (i) a reactor steel; (ii) polytetrafluorethylene (PTFE, trade names Teflon, Hostaflon). The steady state measurements of thermal conductivity were performed at the PTB (Physikalisch Technische Bundesanstalt, Braunschweig, Germany) who guaranteed an absolute accuracy of 2%. For PTFE the data were taken at two different temperatures (see Table 1) and linearly interpolated. The diffusivities were calculated using the specific heat measured by DSC (Perkin Elmer DSC II) and the density. For the reactor steel a recommended interpolation polynom exists between the data points given in the table. As Table 1 shows, the agreement of the data is quite good and the overall absolute accuracy is about 5% with a slight tendency to systematically lower values.

4. REPRESENTATIVE RESULTS

4.1. *PVC*

The polymer polyvinylchloride (PVC: CH_3-$[CH_2CHCl]_n$-CH_3) is an amorphous polymer. At

room temperature it is in the glassy state ($T_g = 90°C$). For numerous applications because of its brittleness it is mostly filled with carbon black to improve shock absorbing. We have used such pieces for testing our data evaluation and the boundary conditions.

4.2. *Rubber*

Rubbers are polymers in the liquid state (melt) hindered to flow by crosslinking. Their well-known tensile properties are due to entropy elasticity. The determination of the associated chain orientation is easily performed measuring birefringence in the case of transparent samples. Like PVC, rubbers are mostly filled (e.g. carbon black, caoline, silica, rutile) for using them in daily surroundings. The chain orientation of such samples is very difficult to measure. The isotherm-method producing ellipses was the first to reveal the magnitude of the anisotropy and, thus, of the chain orientation obtained. It is still more sensitive than measuring two directions separately. This is clear from our measurements. Anisotropy ratios $A \leqslant 1.2$ can only be measured if in each direction the absolute value is known to better accuracy then 10%. The filled rubbers tend to higher orientations than unfilled ones [10].

4.3. *PE*

Polyethylene (polymethylene) is chemically a very simple linear polymer $H_3C\text{-}[\text{-}CH_2\text{-}]_n\text{-}CH_3$. However, like all polymers prepared from the melt it only partly crystallizes (volume crystallinity $0.44 < X_c < 0.82$). The superstructures and morphologies depend on numerous factors. Reproducible are especially oriented states with draw ratios $\lambda = L/L_0 > 3$–4, where L_0 is the initial length and L the actual length. The reason is a structural transformation including melting-recrystallization processes prior to that stage [11]. Thus, the structure produced depends to a large extent only on temperature of the drawing. The overall chain orientation is then uniquely related to the draw ratio. The heat conduction anisotropy for low draw ratios has been investigated by the originally isotherm measurement [8]. Now with the advent of ultra-high molecular weight PE (linear low density PE, $X_c \sim 0.6$) and the procedure of drawing dried gels, where the molecules are largely disentangled, much higher draw ratios and orientations are possible. A macroscopic Young's modulus of half or even two third of the crystals chain modulus (300 GPa) has been obtained. One could expect that the thermal conductivity would rise spectacularly as well. We have measured two series of PE from different sources [12]. The samples were strips of 3–10 mm wide and 50–200 μm thick. The $T(t)$-curves could generally be fitted by the two-dimensional solution. The results are depicted together with measurements on usually drawn low density PE in Fig. 13. The strong increase up to a factor 50 compared to the isotropic value gives hope to the preparation of samples with a unidirectional heat conduction in excess of 50 W/mK i.e. in the range of steel.

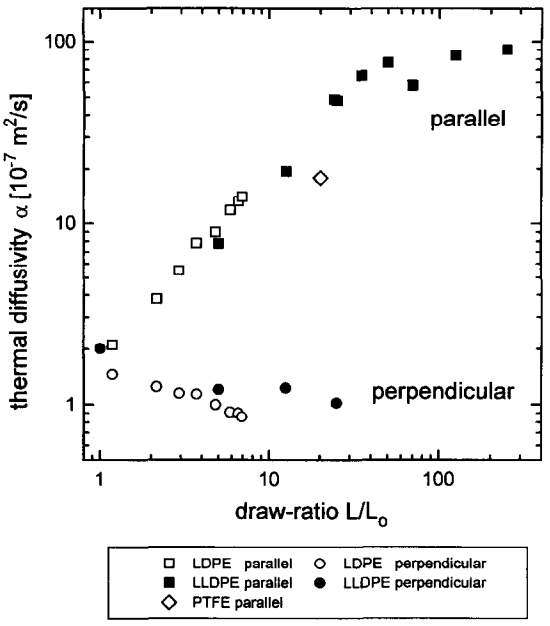

Fig. 13. Thermal diffusivity of oriented polyethylene (PE) and PTFE as a function of draw ratio.

4.4. *PTFE*

Polytetrafluorethylene is just like PE with the hydrogen atoms replaced by fluor atoms. Because of their size, steric hindrances force the all *trans* chains to twist, building a 13/6 helix for $T < 19°C$ and a 15/7 helix at temperatures above 30°C. Since helices generally have lower chain moduli a smaller maximum heat conduction can be expected, however, the helix is forced by steric hindrances of the fluor atoms. This stressed configuration may have rather high chain moduli. Our measurements on an ultraoriented PTFE sample* to our surprise gave a chain direction thermal diffusivity comparable to that of PE. The value is displayed in Fig. 13.

5. CONCLUSION

The method presented is valuable in the case of slab-like geometries of bad conductors with even rough surfaces as in the case of rubbers, where oxygen quickly mars a freshly prepared surface. In the two-dimensional case the thin samples may even show some wavyness like the highly stretched PE samples. Using a line source instead of a point source for heating the probe a better signal-to-noise ratio can be obtained. The lower power density of the line source enables measurements of samples with a low thermal stability. The data analysis represented enables a reliable determination of the absolute thermal diffusivity.

*Supplied by T. Kanamoto/Tokyo.

REFERENCES

1. Fournier, D. and Roger, J. P. (Eds.), 8th International topical meeting on photoacoustic and photothermal phenomena, Point-a-Pitre (Guadeloupe), 22.–25.01.1994. *Journal De Physique*, 1994, **IV**(4), Colloque C7.
2. De Sénarmont, H., Über die Wärmeleitung in kristallisierten Substanzen. *Pogg. Ann.*, 1848, **73,** 191.
3. De Sénarmont, H., Versuche über die Abänderung, welche die mechanischen Agentien der Wärmeleitfähigkeit homogener Körper einprägen. *Pogg. Ann.*, 1849, **76,** 119.
4. Touloukian, Y. S., Powell, R. W., Ho, C. Y. and Klemens, P. G., *Thermophysical Properties of Matter II: Thermal Conductivity of Nonmetallic Solids*. Plenum Press, New York, 1970.
5. Blum K., Kilian H-G. and Pietralla, M., A method for measuring the anisotropy ratio of the thermal conductivity of anisotropic solids. *Journal of Physics E; Science Instruments*, 1983, **16**.
6. Voigt, W., *Lehrbuch der Kristallphysik*. Teubner, Berlin, 1966.
7. Hellmuth, W., Kilian, H-G., Müller, F. H., Kolloid ZuZ polym 218. *Journal of Polymer Science*, 1967, **20**.
8. Kilian, H-G. and Pietralla, M., Anisotropy of thermal diffusivity of uniaxially stretched polyethylenes. *Polymer* 1978, **19**.
9. Chang, Y. P., Kang, C. S. and Chen, D. J., The use of fundamental Green's functions for the solution of problems of heat conduction in anisotropic media. *International Journal of Heat and Mass Transfer*, 1973.
10. Mergenthaler, D. B., Pietralla, M. and Kilian, H.-G., Filler-matrix coupling in rubbers as revealed by heat conduction experiments. *Progress in Colloidal Polymers Science*, 1987, **75**.
11. Heise, B., Kilian, H.-G. and Pietralla, M. Orientation–strain relations in partially crystallized polymers. *Progress in Colloidal Polymer Science*, 1977, **62**.
12. Mergenthaler, D. B., Pietralla, M. and Roy, S., Thermal conductivity in ultraoriented polyethylene. *Macromolecules*, 1992, **25**.
13. Binkele, L., *Fachausschubericht*, Nr.28. Austenitischer chromnickelstahl als standardreferenzmaterial bei messungen der wärme und temperaturleitfähigkeit. Deutsche Keramische Gesellschaft, Köln, 1990.